

# Integrative multi-omics analysis reveals systemic and intestinal responses to heat stress in finishing pigs

Min-Ki Seok<sup>1</sup>, Chiwoong Lim<sup>1</sup>, Young-Jun Seo<sup>1</sup>, Ji-Yeong Lee<sup>1</sup>, Hyunjin Kyoung<sup>2</sup>, Minho Song<sup>2\*</sup>, Jun-Mo Kim<sup>1\*</sup>

<sup>1</sup>Department of Animal Science and Technology, Chung-Ang University, Anseong, Korea

<sup>2</sup>Department of Animal Science and Biotechnology, Chungnam National University, Daejeon, Korea



Received: Sep 25, 2025  
Revised: Oct 24, 2025  
Accepted: Nov 12, 2025

#### \*Corresponding author

Minho Song  
E-mail: mhsong@cnu.ac.kr

Jun-Mo Kim  
E-mail: junmokim@cau.ac.kr

Copyright © 2026 Korean Society of Animal Science and Technology. This is an Open Access article distributed under the terms of the Creative Commons Attribution Non-Commercial License (<http://creativecommons.org/licenses/by-nc/4.0/>) which permits unrestricted non-commercial use, distribution, and reproduction in any medium, provided the original work is properly cited.

#### ORCID

Min-Ki Seok  
<https://orcid.org/0000-0002-4906-0114>  
Chiwoong Lim  
<https://orcid.org/0000-0002-6272-4464>  
Young-Jun Seo  
<https://orcid.org/0000-0001-7520-7733>  
Ji-Yeong Lee  
<https://orcid.org/0000-0002-0775-7191>  
Hyunjin Kyoung  
<https://orcid.org/0000-0001-5742-5374>  
Minho Song  
<https://orcid.org/0000-0002-4515-5212>  
Jun-Mo Kim  
<https://orcid.org/0000-0002-6934-398X>

#### Competing interests

No potential conflict of interest relevant to this article was reported.

#### Abstract

Heat stress (HS) is a major environmental threat to swine production that impairs growth performance and health. Because of their limited thermoregulatory capacity, pigs are highly vulnerable to HS, which results in compromised intestinal integrity, systemic inflammation, and metabolic inefficiency. To elucidate the mechanisms underlying HS acclimation in pigs, we conducted a longitudinal multi-omics analysis integrating fecal microbiome, whole-blood transcriptome, and immune cell deconvolution in finishing pigs under thermoneutral (TN) or HS conditions. HS markedly reduced the average daily gain and feed intake. Microbiome profiling revealed condition-specific shifts: TN pigs showed enrichment of short-chain fatty acid (SCFA)-producing genera, such as *Prevotella* and *Streptococcus*, whereas HS pigs exhibited increased *Clostridium sensu stricto* 1. Functional predictions indicated preservation of the antioxidant and immunomodulatory pathways (glutathione, retinol, and aminoacyl-tRNA biosynthesis) in TN pigs, whereas HS pigs displayed branched-chain amino acid catabolism, reflecting metabolic acclimation under stress. Transcriptomic analysis revealed acute changes at week 1, with 516 differentially expressed genes enriched in hematopoiesis, focal adhesion, cytoskeletal remodeling, and thyroid hormone signaling. By Week 2, these gene responses had declined, suggesting partial acclimation. Network analysis identified cytoskeletal genes (*ACTB*, *MYL9*, *ACTN4*, and *COL4A4*) as the central regulators. Immune deconvolution further showed the HS-driven elevation of cytotoxic T and myeloid subsets, in contrast to B cell populations which were maintained under TN, highlighting divergent immune trajectories. Integration of the microbiome, transcriptome, and immune data revealed two axes: (1) cytotoxic T cells positively associated with *Clostridium sensu stricto* 1, but negatively associated with cytoskeletal genes, and (2) B cells positively linked to *Prevotella*, *Lactobacillus*, and structural genes. Only the B-cell structural axis formed a coherent cross-layer module, indicating a recovery-oriented response. These findings demonstrate that resilience to HS requires the coordination of humoral immunity, cytoskeletal reinforcement, and SCFA-producing microbiota. The identified biomarker axis (*Prevotella*, B cells, and cytoskeletal genes) provides a mechanistic basis for developing precise strategies to enhance thermal tolerance in swine.

**Keywords:** Heat stress, Finishing pigs, Multi-omics integration, Cell deconvolution

### Funding sources

This work was supported by the National Research Foundation of Korea (NRF) grant funded by the Korea government (MSIT) (RS-2022-NR069268). This research was supported by the Chung-Ang University Graduate Research Scholarship (Academic scholarship for College of Biotechnology and Natural Resources) in 2023.

### Acknowledgements

Not applicable.

### Availability of data and material

Upon reasonable request, the datasets of this study can be available from the corresponding author.

### Authors' contributions

Conceptualization: Kim JM, Song M.  
Data curation: Seok MK.  
Formal analysis: Seok MK.  
Methodology: Lim C, Seo YJ, Kyoung H.  
Software: Lim C, Seo YJ, Lee JY.  
Validation: Seok MK.  
Investigation: Seok MK.  
Writing - original draft: Seok MK.  
Writing - review & editing: Seok MK, Lim C, Seo YJ, Lee JY, Kyoung H, Song M, Kim JM.

### Ethics approval and consent to participate

This research was approved by the Institutional Animal Care and Use Committee (IACUC) of Chungnam National University (202012A-CNU-204).

### Declaration of generative AI

No AI tools were used in this article.

## INTRODUCTION

As the global expansion of the swine industry continues, heat stress (HS) driven by climate change has emerged as a critical challenge [1]. Compared to other livestock species, pigs are particularly vulnerable to elevated ambient temperatures due to their insufficiently developed sweat glands and substantial subcutaneous adipose tissue, both of which significantly limit effective thermoregulation [2]. Physiologically, HS induces peripheral vasodilation, reduces blood flow to the visceral organs, and compromises intestinal health [3]. The resulting intestinal hypoxia subsequently weakens the gut barrier integrity and facilitates pathogen translocation and systemic inflammation [4]. Additionally, HS negatively affects swine productivity and profitability, thereby causing reduced feed intake, impaired growth performance, and decreased reproductive efficiency, particularly during the finishing pig stage of the high growth phase [5,6].

Despite extensive studies investigating the HS responses in swine, comprehensive research utilizing multiomics integration (MOI) approaches to elucidate the underlying biological mechanisms remains limited [7]. HS simultaneously influences diverse physiological pathways, including immune, metabolic, and intestinal homeostasis pathways, through intricate host-microbiome interactions, leading to systemic pathological outcomes [8,9]. Previous single-omics studies have further provided limited insights into these relationships. Typically, transcriptomic analyses offer only an incomplete understanding of gene regulatory mechanisms without adequately addressing microbiome interactions [10]. Conversely, microbiome-centric studies have independently elucidated shifts in microbial composition associated with gut barrier function, immunity, and metabolism, but have failed to clarify the direct molecular implications on systemic physiological responses [11]. Therefore, an MOI approach is essential to bridge these fragmented insights by correlating microbial community shifts with host gene expression, thereby enabling the simultaneous investigation of systemic and intestinal responses to HS [12,13]. To ensure analytical robustness, it is essential to collect biospecimen-derived data that accurately represents distinct biological layers of the host [14]. Accordingly, fecal and whole blood samples were used to noninvasively and longitudinally evaluate host physiological responses to HS, highlighting their utility for the real-time assessment of intestinal and systemic alterations.

Conventional bulk blood transcriptomics have a critical limitation: HS remodels immune cell populations, and bulk profiles may conflate compositional shifts with intrinsic gene regulatory changes. To address this issue, we applied cell-type deconvolution, which disentangles population dynamics from transcriptional regulation, and refines the resolution of immune acclimation under HS [15]. Collectively, this study employed an MOI framework combining microbiome, transcriptome, and immune cell data to comprehensively characterize the systemic and intestinal responses of finishing pigs to HS. We hypothesized that integrating these multilayered data would reveal condition-specific host-microbiome-immune system interaction axes, thereby uncovering the mechanistic pathways underlying acclimations or malacclimations to HS. This integrative approach aims to not only advance the understanding of swine thermal stress biology but also to provide a conceptual basis for precise strategies to enhance resilience in the swine industry.

## MATERIALS AND METHODS

### Ethics statement

All experimental protocols were approved by the Institutional Animal Care and Use Committee (Approval No. 202012A-CNU-204) of Chungnam National University, Daejeon, South Korea. All animal handling and sampling procedures were conducted in accordance with animal use guidelines

and regulations.

### Temperature and humidity index

The temperature and humidity index (THI) was calculated using the formula suggested by the NRC [16]:

$$\text{THI} = (1.8 \times \text{Tdb} + 32) - [(0.55 - 0.0055 \times \text{RH}) \times (1.8 \times \text{Tdb} - 26.8)]$$

where Tdb is the dry-bulb temperature and RH is the relative humidity.

### Experimental design, animals, and diets

This experiment followed a two-factor factorial design consisting of two environment treatments (thermoneutral, TN; and HS) and three time points (Weeks 0, 1, and 2). Twenty-four crossbred finishing pigs ([Landrace x Yorkshire] × Duroc; initial body weight, BW = 51.14 ± 5.79 kg; 12 TN and 12 HS) were assigned to two environmental treatments in a randomized complete block design (block = BW) during 14 days. Both fecal microbiome and whole-blood transcriptome data were generated from all individuals at each time point. Environmental treatments were as follows: ① THI 68 (comfort); 23°C–24°C, 35% and ② THI 87 (severe); 32°C–33°C, 80%, and were designed based on previous reports [17]. Pigs were fed a basal diet (corn-soy diet; 3,350 kcal/kg ME; 18.55% CP; 1.23% lysine; 0.38% methionine) formulated to meet or exceed the nutrient requirements of growing pigs (NRC, 2012; table 2.1) [18]. Pigs were provided ad libitum access to feed and water throughout the experimental period. Each pen size was 2.32 × 1.75 × 0.7 m. The pen floor was slatted with 100% plastic.

### Growth performance measurement and statistical analysis

Body weights were recorded at the start and end of the 14-day experimental period. Average daily gain (ADG), average daily feed intake (ADFI), and gain-to-feed ratio (G:F) were subsequently calculated. Statistical analyses were conducted using independent sample *t*-tests with the SAS 9.4 statistical software package (SAS Institute). Data are presented as the mean ± SEM, with significance thresholds set at  $p < 0.05$  and  $p < 0.01$ .

### 16S rRNA sequencing library preparation

Genomic DNA was extracted from fecal samples to amplify the V3–V4 hypervariable regions of the bacterial 16S rRNA gene following the Illumina 16S Metagenomic Sequencing Library Preparation protocol. Each reaction contained 2ng of template DNA, 5×reaction buffer, 1mM dNTPs, 500 nM of each universal primer, and Herculase II Fusion DNA Polymerase (Agilent Technologies). The PCR cycling conditions consisted of an initial denaturation at 95°C for 3 min, followed by 25 cycles of denaturation at 95°C for 30 s, annealing at 55°C for 30 s, and extension at 72°C for 30 s, with a final extension step at 72°C for 5 min. The forward primer sequence was: 5'-GTCGGCAGCGTCAGATGTGTATAAGAGACAGCCTACGGGNGGCWGC AG-3', and the reverse primer sequence was 5'-GTCTCGTGGGCTCGGAGATGTGTATAAGA GACAGGACTACHVGGGTATCTAATCC-3'. PCR products were purified using AMPure XP beads (Beckman Coulter). A secondary PCR of 10 cycles was subsequently conducted to attach the Nextera XT index sequences and Illumina sequencing adapters, followed by a second purification step using AMPure XP beads. The concentrations of the indexed libraries were quantified using the KAPA Library Quantification Kit (KAPA Biosystems), while the fragment size distribution was verified using the Agilent TapeStation D1000 system. Paired-end sequencing (2 × 300 bp) was

performed using the Illumina MiSeq platform (Illumina) at Macrogen.

### **Microbiome data analysis and taxonomy classification**

Raw paired-end reads were processed using the QIIME2 platform v2024.2 to characterize the fecal microbial community [19]. After demultiplexing and initial quality filtering, sequences were denoised using the DADA2 algorithm to correct amplicon errors and generate high-resolution amplicon sequence variants (ASVs) [20]. Taxonomic classification of these ASVs was conducted using a Naïve Bayes classifier trained on the SILVA v138\_99 database specific to the V3–V4 region of the 16S rRNA gene [21]. The alpha diversity within each sample was assessed using the observed ASV counts and Shannon diversity indices, whereas beta diversity between samples was evaluated based on the Bray–Curtis dissimilarity and visualized using nonmetric multidimensional scaling (NMDS). Statistical comparisons of beta diversity among groups were performed using permutational multivariate analysis of variance (PERMANOVA). This taxonomic framework allowed for the profiling of microbial communities from the phylum to the genus level across treatment groups and sampling times.

### **Functional prediction of microbial communities**

The functional potential of the fecal microbiota was inferred using phylogenetic investigation of communities through reconstruction of unobserved state 2 (PICRUSt2) [22]. The ASV tables were normalized to the 16S rRNA gene copy numbers prior to functional inference. The predicted enzyme commission (EC) numbers and Kyoto Encyclopedia of Genes and Genomes (KEGG) orthologs were assigned based on the PICRUSt2 reference database. These functional annotations were subsequently mapped to the KEGG pathways to facilitate the interpretation of metabolic capabilities. Statistical comparisons between the experimental groups were conducted using Welch's *t*-test within the statistical analysis of taxonomic and functional Profiles (STAMP) software [23], with a significance level of  $p < 0.05$ . Extended error bar plots generated by STAMP were applied to visualize the significantly different pathways, providing a comparative overview of the predicted metabolic functions under distinct environmental conditions.

### **RNA extraction, library preparation, and sequencing**

Total RNA was isolated from whole blood samples using TRIzol reagent (Invitrogen, Life Technologies), following the manufacturer's protocol, to ensure RNA integrity and minimize degradation. The concentration and purity of each RNA sample were assessed using a NanoDrop ND-1000 spectrophotometer (NanoDrop Technologies). For RNA-seq library construction, 1 µg of total RNA was processed using the Illumina TruSeq RNA Sample Preparation Kit. In brief, mRNA was fragmented and reverse-transcribed into first-strand complementary DNA (cDNA) using reverse transcriptase and random primers. Second-strand synthesis was performed using DNA polymerase I and ribonuclease H to obtain double-stranded cDNA. End-repair and adapter ligation were conducted to complete the library construction. The resulting libraries were sequenced on an Illumina HiSeq 2000 platform (Illumina) to generate 2 × 100 bp paired-end reads, thereby enabling comprehensive transcriptome profiling for downstream analysis.

### **Data processing and differentially expressed gene identification**

Raw RNA-seq reads were initially assessed for quality using FastQC v0.11.9, to identify potential sequencing artifacts and base-calling errors [24]. Low-quality bases and residual adapter sequences were removed with Trimmomatic v0.38 using a sliding window approach (SLIDING WINDOW:4:15) with a minimum read length threshold of 80 bp [25]. The trimmed reads were

subsequently re-evaluated using FastQC v0.11.9 to confirm the quality improvement. High-quality reads were aligned to the *Sus scrofa* reference genome (Sscrofa11.1, Ensembl release 111) using HISAT2 v2.1.0, with default alignment parameters [26]. Gene annotation was performed based on the corresponding Ensembl GPF file. The resulting SAM files were converted to the BAM format, sorted, and indexed using Samtools v1.9 [27]. Gene-level read counts were generated using the FeatureCounts tool in the Subread package v1.6.3, by employing the corresponding Ensembl GTF annotation file [28]. Raw counts were normalized using the trimmed mean of M-values (TMM) method implemented in the edgeR package in Bioconductor v3.16 to account for differences in library size [29]. Multidimensional scaling (MDS) plots were generated using the Limma package to visualize sample relationships, while graphical outputs were produced using ggplot2 [30]. Differentially expressed genes (DEGs) were identified by comparing the TN and HS groups at each time point (Weeks 0, 1, and 2), with significance defined as a false discovery rate (FDR) < 0.05 and an absolute  $\log_2$  fold change  $\geq 1$ , applying the Benjamini-Hochberg correction for multiple testing.

### Functional enrichment analysis

Functional enrichment analysis was conducted to investigate the biological roles of the identified DEGs. Gene ontology (GO) enrichment, focusing on the biological process category, was conducted using DAVID v2021, with a minimum gene count of two and an EASE score threshold of  $p < 0.05$  [31]. Redundant GO terms were summarized and visualized as tree maps using the reduced visualization gene ontology (REVIGO) [32]. KEGG pathway analysis was conducted to identify overrepresented molecular pathways, and the results were presented as  $-\log_{10}$   $p$ -values and fold enrichment values. To further interpret the relationships among functional categories, selected DEGs were integrated into network analyses using the Cytoscape v3.10.0, ClueGO v2.5.10, and CluePedia v1.5.10 plugins [33–35]. Network construction employed a  $p$ -value cut-off of < 0.05, and the ClueGO parameters were set as follows: GO term minimum level = 3, maximum level = 8, minimum number of genes = 3, and minimum gene percentage = 4%. This approach enabled the identification of key regulatory modules and functional clusters associated with the HS response.

### Cell-type deconvolution

Immune cell composition was estimated from whole blood transcriptomic data using the xCell2 algorithm, which applies cell type-specific gene expression signatures to calculate enrichment scores [36]. The TMM-normalized gene expression matrix generated from the RNA-seq analysis served as the input for cell-type deconvolution. The default immune reference compendium provided by xCell2 was applied to profile 40 predefined immune cell types, including subsets of T cells, B cells, and monocytes. The resulting enrichment scores were subsequently compared between TN and HS groups to identify shifts in the immune landscape. These immune cell profiles were then integrated with the microbiome and transcriptome data for multi-omics analysis to elucidate host-microbiome-immune system interactions under HS conditions.

### Multi-omics integration

To investigate the coordinated interactions between the fecal microbiome and host immune responses under HS, MOI was conducted using regularized canonical correlation analysis (rCCA) and Mantel tests. For rCCA, microbial abundance data were log-ratio transformed, and TMM-normalized gene expression matrices representing immune-related features were prepared. Both datasets were standardized to have a zero mean and unit variance prior to the analysis. rCCA was conducted using the CCA function from the PMA package v1.2.1 in R, identifying canonical variates that maximized

correlations between microbial and host immune features [37]. Canonical loadings were extracted and ranked to identify the most influential microbial taxa and immune cell types.

Mantel tests were applied to evaluate the correlations between the distance matrices derived from different omics layers. Bray–Curtis dissimilarity was used for microbial profiles, whereas Euclidean distances were calculated for both transcriptomic and cell-type deconvolution data. Significance was determined through permutation testing with 9,999 iterations using the Mantel\_test function from the linkET package v0.0.1 in R [38]. This integrated framework enabled the identification of microbiome–immune associations and functional modules characteristic of the HS response.

## RESULTS

### Growth performance under HS

At the start of the experiment, the initial body weight did not differ significantly between the TN groups ( $53.37 \pm 1.49$  kg) and HS groups ( $50.61 \pm 4.01$  kg,  $p > 0.05$ ). However, after exposure, the HS pigs showed markedly lower ADG ( $0.48 \pm 0.03$  vs.  $0.81 \pm 0.04$  kg/d) and ADFI ( $1.17 \pm 0.02$  vs.  $1.89 \pm 0.05$  kg/d) than TN pigs ( $p < 0.01$ ). However, no significant differences were found in the G:F ( $0.41 \pm 0.02$  vs.  $0.43 \pm 0.03$ ,  $p > 0.05$ ) between groups. These results suggest that HS reduced growth performance, primarily through reductions in feed consumption and weight gain, rather than in feed efficiency (Table 1).

### HS-driven shifts in fecal microbiota composition and function

Fecal microbiome analyses revealed marked compositional and functional alterations under HS conditions. Alpha diversity metrics, including the observed ASV counts and Shannon index, remained statistically unchanged across treatment groups and time points (weeks 1 and 2), indicating that within-sample diversity was unaffected by HS (Fig. 1A). In contrast, the beta diversity analysis based on Bray–Curtis dissimilarities displayed distinct clustering of microbial communities according to the treatment, with clear group separation in both weeks (Fig. 1B). This pattern indicated that HS primarily influenced the overall microbial structure, rather than species richness.

At the genus level, the microbiota composition differed according to treatment. *Prevotella* and *Streptococcus* were more abundant in TN pigs, whereas *Clostridium sensu stricto* 1 was elevated in the HS group (Fig. 1C). The *Firmicutes*:*Bacteroidota* (F:B) ratio was significantly higher in the 1\_HS group than in the 1\_TN ( $p < 0.05$ ), indicating a transient phylum-level imbalance in response to acute HS. This difference dissipated by week 2, when the F:B ratios returned to comparable levels between groups (Fig. 1D), indicating a potential microbial acclimation [8].

Functionally, PICRUSt2-based metagenomic inference showed divergent metabolic profiles

**Table 1.** Growth performance of pigs under heat stress

Group	Body weight (kg)		Average daily gain (kg/d)	Average daily feed intake (kg/d)	Gain:feed ratio (G:F)
	Week 0	Week 2			
TN	$53.37 \pm 1.49$	$64.65 \pm 1.33$	$0.81 \pm 0.04^{**}$	$1.89 \pm 0.05^{**}$	$0.43 \pm 0.03$
HS	$50.61 \pm 4.01$	$57.35 \pm 4.14$	$0.48 \pm 0.03^{**}$	$1.17 \pm 0.02^{**}$	$0.41 \pm 0.02$

Each value represents the mean of four pigs per treatment (one pig/pen).

<sup>\*\*</sup> $p < 0.01$ .

SEM, standard error of the mean; TN, thermoneutral; HS, heat stress.

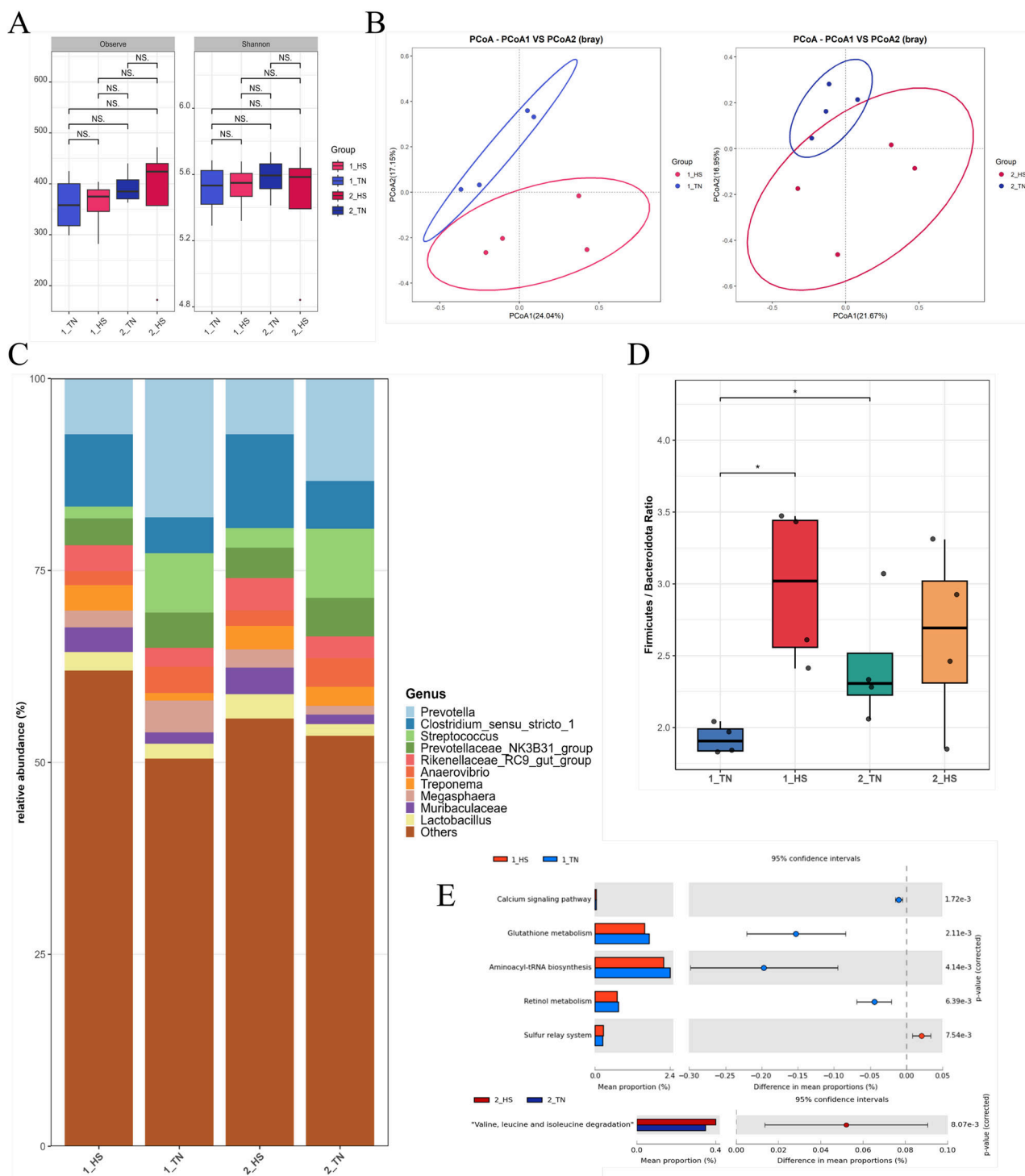


**Fig. 1. Fecal microbiome responses in finishing pigs under heat stress (HS).** (A) Alpha diversity metrics, including observed species richness and Shannon diversity index, were compared between the thermoneutral (TN) and HS groups in Weeks 1 and 2, with no significant differences detected via the Kruskal–Wallis test. (B) Principal coordinate analysis (PCoA) based on Bray–Curtis dissimilarities showed clear compositional separation between the TN and HS pigs at both time points. (C) The genus-level composition of the fecal microbiota revealed the ten most abundant taxa across groups, visualized as the mean relative abundance per treatment. (D) The F:B ratio was calculated to assess the phylum-level shifts associated with heat exposure. (E) Functional profiles inferred via phylogenetic investigation of communities through reconstruction of unobserved state 2 (PICRUSt2) indicated group-specific pathway activity, with the left panel displaying average Kyoto Encyclopedia of Genes and Genomes (KEGG) pathway abundances per group, and the right panel showing intergroup differences with 95% confidence intervals; pathways enriched in TN and HS pigs are presented in blue and red, respectively.

between treatments. At Week 1, TN pigs exhibited enrichment of glutathione metabolism, retinol metabolism, and aminoacyl-tRNA biosynthesis pathways, reflecting a preserved redox balance and protein synthesis capacity under non-stressed conditions [39–41]. Conversely, at week 2, the HS group showed an increased representation of the valine, leucine, and isoleucine degradation pathways, implicating the adaptive catabolism of branched-chain amino acids under prolonged stress (Fig. 1E) [42].

### RNA-seq quality metrics

RNA-Seq generated an average of 39.3 million raw reads per sample. After trimming, approximately 38.5 million high-quality reads per sample were retained, with minimal sequence loss (mean trimming rate: 1.9%) and consistent GC content (approximately 44.3%). The read alignment yielded a mean uniquely mapped rate of 85.3% and an overall mapping rate of 96.7%, thus confirming the reliability of the sequencing data for transcriptome analysis (Table 2).

### Temporal dynamics of gene expression changes

The MDS plots demonstrated clear treatment-driven clustering between TN and HS samples,

**Table 2.** Overview of the transcriptome data processing

Group	Sample name	Raw			After trimming				After mapping	
		Total	Sequence length	GC (%)	Remaining reads after trimming	Sequence length trimmed (bp)	Trimmed GC (%)	Trimming rate (%)	Uniquely mapped rate (%)	Overall mapped rate (%)
TN	F0.T1.104.A	40,015,742	101	44	39,205,704	36–101	44	2.02	86.74	97.09
	F0.T1.110.B	36,655,351	101	45	35,968,868	36–101	45	1.87	88.31	96.87
	F0.T1.34.A	34,174,726	101	44	33,475,035	36–101	44	2.05	87.32	96.81
	F0.T1.97.A	34,637,870	101	46	33,938,438	36–101	46	2.02	86.14	97.05
	F1.T1.104.A	43,914,182	101	44	43,109,613	36–101	44	1.83	85.25	96.88
	F1.T1.110.B	44,427,939	101	44	43,550,608	36–101	44	1.97	84.11	96.87
	F1.T1.34.A	39,689,690	101	44	38,969,075	36–101	44	1.82	84.80	96.49
	F1.T1.97.A	41,154,600	101	43	40,407,367	36–101	43	1.82	85.91	97.07
	F2.T1.104.A	39,273,798	101	44	38,545,142	36–101	44	1.86	84.10	96.67
	F2.T1.110.B	40,638,650	101	44	39,844,878	36–101	44	1.95	83.56	96.50
	F2.T1.34.A	40,749,175	101	44	39,928,436	36–101	44	2.01	84.38	96.87
	F2.T1.97.A	37,606,367	101	45	36,881,186	36–101	45	1.93	84.18	96.49
HS	F0.T4.105.B	37,629,934	101	45	36,788,772	36–101	45	2.24	83.74	96.77
	F0.T4.140.B	35,218,302	101	46	34,480,374	36–101	45	2.1	84.36	96.6
	F0.T4.16.A	41,312,791	101	44	40,563,077	36–101	44	1.81	86.38	96.13
	F0.T4.23.B	44,497,346	101	45	43,623,005	36–101	45	1.96	86.89	96.84
	F1.T4.105.B	36,940,490	101	44	36,284,344	36–101	44	1.78	85.19	96.73
	F1.T4.140.B	42,127,626	101	44	41,278,975	36–101	44	2.01	85.04	96.85
	F1.T4.16.A	37,505,867	101	44	36,795,088	36–101	44	1.90	85.14	96.29
	F1.T4.23.B	40,108,579	101	44	39,350,345	36–101	44	1.89	85.14	97.05
	F2.T4.105.B	38,137,968	101	45	37,410,246	36–101	45	1.91	85.18	96.44
	F2.T4.140.B	37,911,150	101	44	37,291,442	36–101	44	1.63	85.16	96.70
	F2.T4.16.A	38,295,985	101	45	37,609,835	36–101	45	1.79	84.44	96.27
	F2.T4.23.B	39,509,036	101	44	38,845,012	36–101	44	1.68	85.99	96.86

TN, thermoneutral; HS, heat stress.

whereas temporal separation among weeks was relatively subtle (Fig. 2A). At each time point, the TN and HS samples formed distinct clusters, reflecting consistent transcriptional responses to thermal stress (Fig. 2B).

At Week 0, however, no significant differences in gene expression were detected between TN and HS pigs, confirming comparable baseline transcriptional profiles prior to heat exposure (Supplementary Fig. S1). Differential gene expression analysis revealed a robust early phase response. At Week 1, 384 genes were upregulated and 132 were downregulated in HS pigs. By Week 2, the DEG count declined markedly, with only 15 upregulated and 53 downregulated genes (Fig. 2C). This reduction indicates an acute transcriptional response during the initial stress exposure, followed by partial acclimation or resolution.

### Biological pathways enriched in differentially expressed genes

GO enrichment analysis of Week 1 DEGs identified processes, including hematopoiesis, transcriptional activation, mechanical stimulus detection, and cell migration (Fig. 3A), suggesting rapid mobilization of immune and regenerative programs. In Week 2, the enriched GO terms shifted toward metabolic and homeostatic functions, such as oxygen transport and phosphatase regulation (Fig. 3B). KEGG pathway analysis at week 1 further supported these findings, with significant enrichment in thyroid hormone signaling, focal adhesion, gastric acid secretion, and chromatin remodeling pathways (Fig. 3C). No KEGG pathways were significantly enriched at week 2, likely due to the reduced number of DEGs.

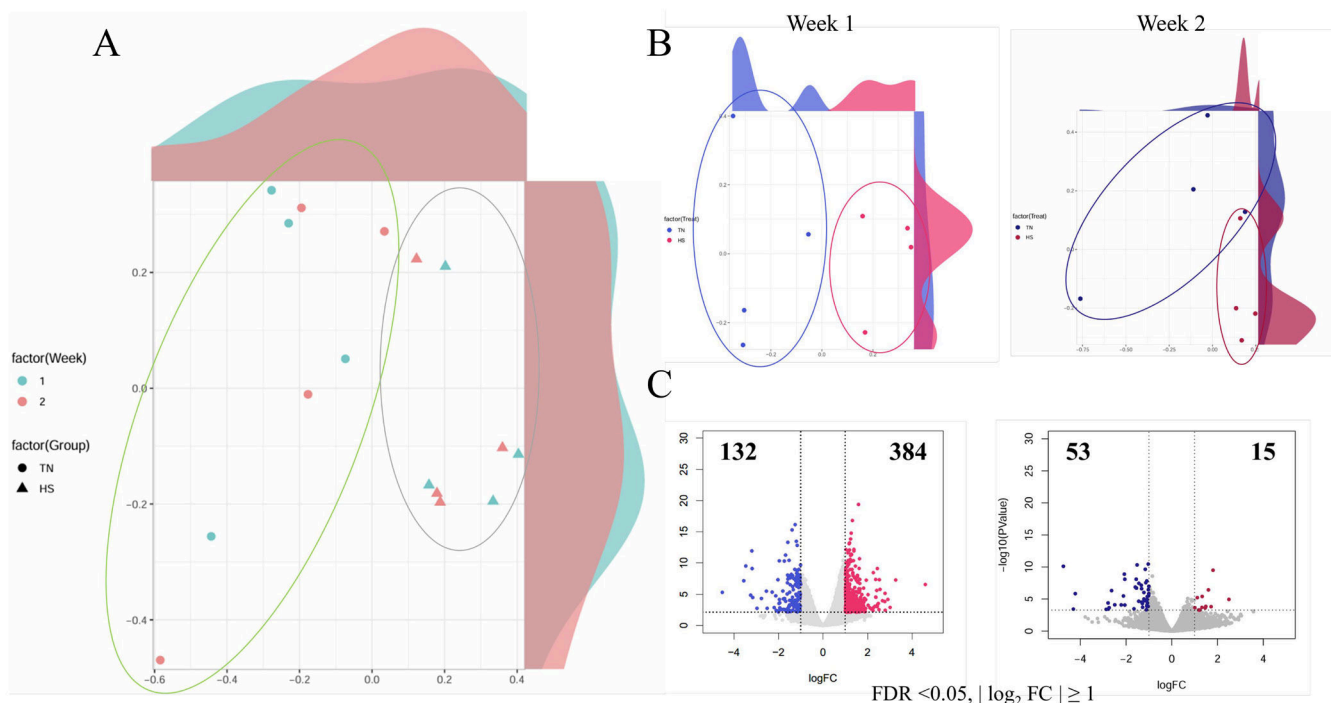


**Fig. 2. Transcriptomic landscape of whole blood in finishing pigs under thermal stress.** (A) Multidimensional scaling (MDS) plot based on variance-stabilized expression profiles across all samples; color distinguishes the sampling week while shape indicates treatment group. (B) MDS plots stratified by week showing clear separation between the thermoneutral (TN; blue) and heat-stressed (HS; red) groups in both Weeks 1 and 2, indicating distinct transcriptomic responses to heat exposure. (C) Volcano plots of differentially expressed genes (DEGs) between HS and TN groups, with significant genes highlighted in red (upregulated) and blue (downregulated) based on  $\text{FDR} < 0.05$  and  $|\log_2 \text{fold change}| > 1$ .

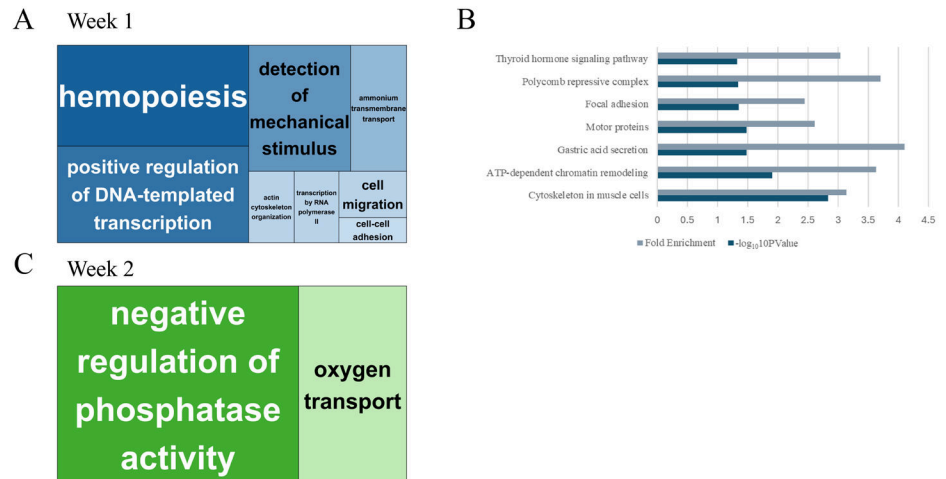


**Fig. 3. Functional enrichment analysis of differentially expressed genes (DEGs) under heat stress (HS).** (A) Gene ontology (GO) biological processes enriched in DEGs from Week 1, visualized using reduced visualization gene ontology (REVIGO). Each box denotes a GO term, with box size indicating the relative specificity and semantic contribution of the term within the enriched set. (B) Kyoto Encyclopedia of Genes and Genomes (KEGG) pathway enrichment analysis for Week 1 DEGs, presenting fold enrichment (dark bars) alongside the statistical significance represented by  $-\log_{10}$ -transformed  $p$ -values (light bars). (C) REVIGO plot summarizing the GO biological processes enriched in DEGs from Week 2, with box dimensions reflecting term relevance and frequency. KEGG pathway analysis for Week 2 was not conducted due to the limited number of DEGs identified.

### Co-expression network analysis

Co-expression network analysis of the Week 1 DEGs using Cytoscape revealed functionally grouped modules, including focal adhesions, cytoskeletal organization, thyroid signaling, and chromatin remodeling (Fig. 4). Additional clusters were associated with disease-related pathways, such as acute myeloid leukemia and basal cell carcinoma, potentially reflecting conserved stress-responsive gene programs. These network structures further highlighted the coordinated regulation of mechanical integrity, signal transduction, and transcriptional dynamics in response to acute HS.

### Immune cell remodeling under thermal challenge

Cell-type deconvolution analysis revealed distinct immune profiles in the TN and HS groups over time (Fig. 5). At Week 1, HS pigs showed an elevated enrichment of multiple T cell subsets, including regulatory and memory CD8<sup>+</sup> and CD4<sup>+</sup> populations, along with myeloid cells. In contrast, TN pigs exhibited greater enrichment of B cell subsets, such as naïve, memory, and plasma B cells, indicating the maintenance of humoral immunity under thermoneutral conditions [43]. At Week 2, the HS samples retained elevated levels of cytotoxic T cells and plasmablasts, indicating sustained cellular immune engagement. TN samples display an increased abundance of natural killer (NK) cell subsets, including regulatory and cytotoxic NK cells, indicating stable innate immune surveillance [44].

### Canonical correlation between microbiota and immune cell types

The rCCA identified distinct patterns of association between microbial genera and immune cell populations under each environmental condition. In the HS group, B cell subsets were positively correlated with *Prevotella*, *Megasphaera*, *Lactobacillus*, and *Butyrivibrio*, suggesting microbial support for humoral immunity. Conversely, T cell subsets exhibited positive correlations with *Clostridium sensu stricto* 1, indicating the potential microbial modulation of cellular immunity under

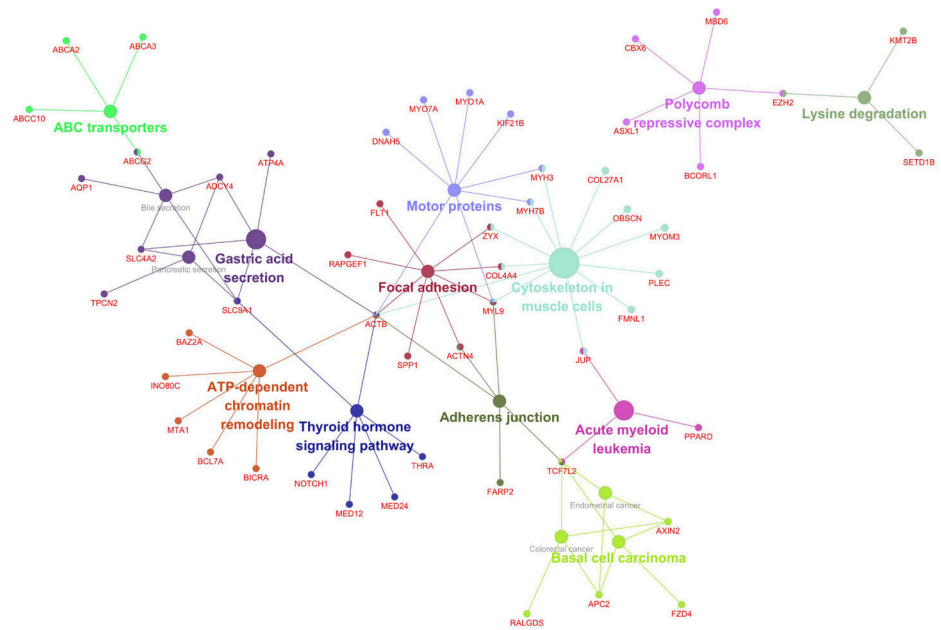


**Fig. 4. Co-expression network of functionally enriched genes responding to heat stress (HS) at week 1.** A gene co-expression network was constructed using differentially expressed genes (DEGs) identified in heat-stressed pigs in Week 1. Functional grouping and visualization were conducted using ClueGO, with the following parameters: gene ontology (GO) term level range set from 3 to 8, a minimum of three genes per term, and a minimum gene contribution of 4.0%. Nodes represent individual genes or enriched GO terms, with the node color reflecting functionally related clusters. Edges indicate co-expression relationships or shared functional annotations among connected genes.

stress (Fig. 6A).

In TN pigs, positive correlations were observed between T cells and genera, such as *Subdoligranulum* and *Holdemania*, whereas *Oscillibacter* and *Parasutterella* were negatively associated with both T cells and eosinophils (Fig. 6B). These contrasting association networks indicate the existence of condition-specific microbiota-immune interactions.

### Multi-layer correlation of microbiota, immune cells, and genes

The integration of gene expression, immune cell composition, and microbial taxa revealed a coordinated molecular framework under HS conditions (Fig. 7). A positively correlated module included B cell subsets and cytoskeletal genes (e.g., *ACTB*, *MYL9*, *COL4A4*, and *ACTN4*), suggesting that structural reinforcement is linked to humoral immunity. In contrast, T-cell subsets showed negative correlations with the same genes, indicating an immune axis shift.

Mantel tests confirmed that genera such as *Prevotella* and *Lactobacillus* were aligned with the B cell-gene module, whereas *Clostridium sensu stricto* 1 and *Megasphaera* were linked to T cell-enriched networks. These results together demonstrate a hierarchical interaction structure that integrates microbial composition with host immune dynamics and transcriptional programs during acclimation to HS.

## DISCUSSION

Overall, the results of this study show that HS significantly impaired growth performance in finishing pigs, as indicated by marked reductions in both average daily gain and feed intake. HS

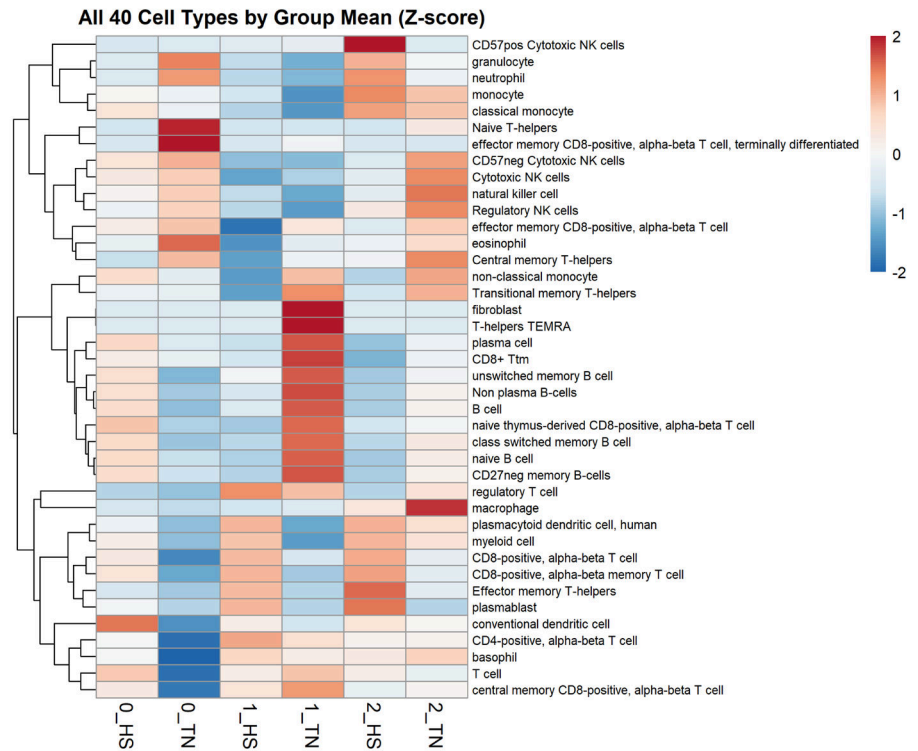


**Fig. 5. Inferred immune cell landscape in peripheral blood across thermoneutral and heat-stressed pigs.** A heatmap showing the standardized enrichment scores (z-scores) of 40 immune and stromal cell types, inferred from bulk RNA-seq data using transcriptome-based deconvolution. Columns represent the mean values for each group at Weeks 0, 1, and 2, while rows correspond to the individual cell types. The color gradient reflects the relative abundance, with red indicating higher enrichment and blue denoting lower levels.

reduced growth performance primarily through decreased feed intake and body-weight gain, without significant changes in feed efficiency, likely due to reduced visceral blood flow, impaired nutrient absorption, and elevated stress hormone levels. These systemic effects are consistent with suppressed anabolic growth and altered energy-utilization pathways.

In addition to these physiological disruptions, substantial changes were observed in the gut microbiota. Principal coordinate analysis revealed a clear divergence in the microbial community structure between the groups over time. Taxonomic profiling revealed that short-chain fatty acid (SCFA)-producing genera such as *Prevotella* and *Streptococcus* were depleted under HS conditions, while *Clostridium sensu stricto* 1 was enriched (Fig. 1C). The loss of *Prevotella* and *Streptococcus* indicates impaired mucosal barrier function and reduced SCFA availability, thereby weakening anti-inflammatory regulation by diminishing SCFA-mediated Treg induction and IL-10 production [45,46]. In contrast, the increase in *Clostridium sensu stricto* 1, associated with branched-chain amino acid (BCAA) fermentation and cytotoxic byproduct production, may exacerbate epithelial damage and inflammation [47]. Consistent with these compositional changes, the predicted microbial pathways in TN pigs were enriched in antioxidant (glutathione), immunomodulatory (retinol), and translational (aminoacyl-tRNA biosynthesis) processes. In contrast, HS pigs showed a diminished representation of these pathways, while protein catabolism via BCAA degradation became more prominent by week 2, indicating a stress-adaptive shift in energy utilization that may contribute to an increased nitrogenous burden and barrier disruption [42].

At the host level, transcriptomic profiling revealed strong time-dependent changes in gene

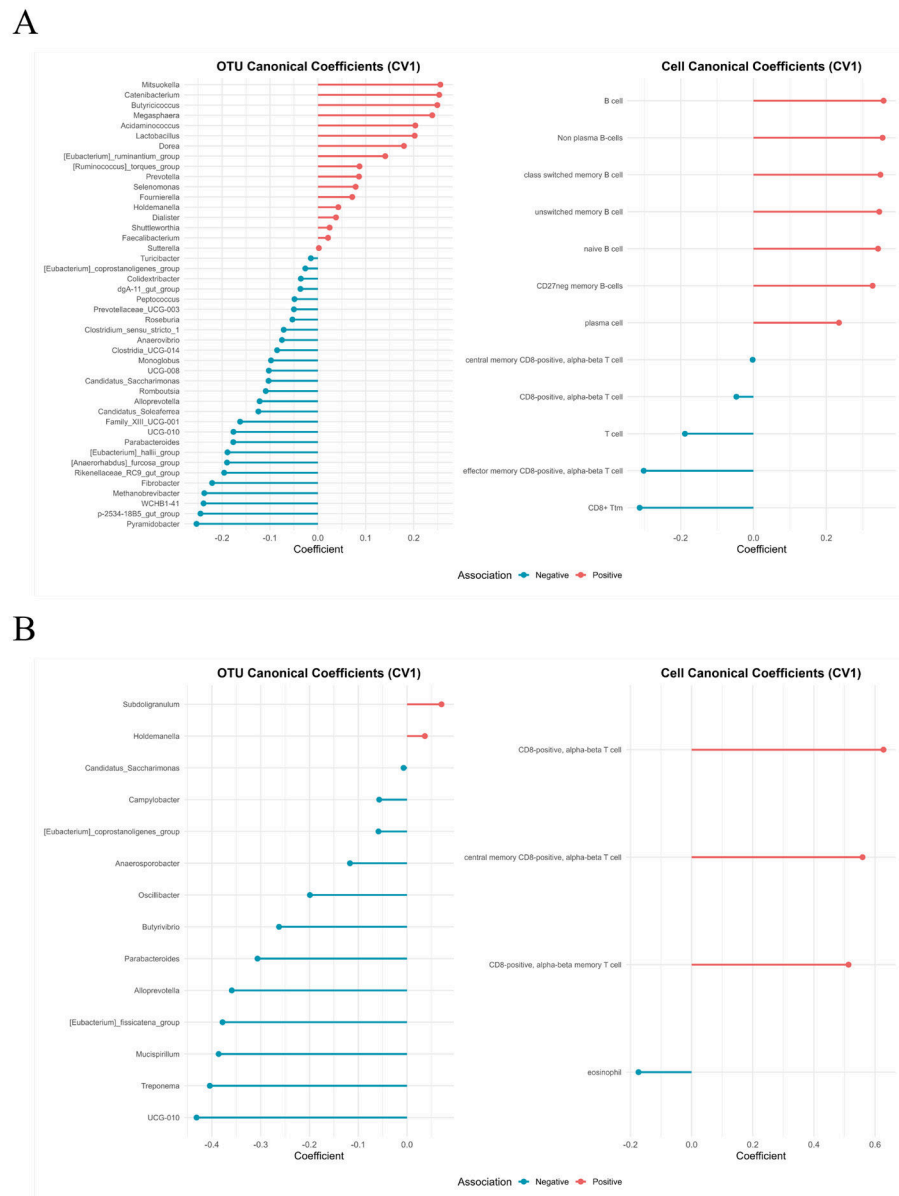


**Fig. 6. Regularized canonical correlation analysis (rCCA) showing distinct host–microbiome association patterns under heat stressed and thermoneutral conditions.** Canonical correlation analysis using rCCA illustrates the differential correlation structure between fecal microbial genera and peripheral immune cell subsets in (A) heat-stressed and (B) thermoneutral pigs. Bar plots present the canonical coefficients of the first variate (CV1), with microbial taxa shown on the left and immune cell types on the right. Red and blue bars indicate positive and negative associations, respectively, with longer bars denoting greater contributions to the multivariate correlation structure.

expression. A pronounced response occurred during week one, with enrichment of biological processes related to hematopoiesis, transcriptional regulation, and immune cell trafficking. By week two, the response was attenuated, indicating partial resolution or acclimation. GO and KEGG analyses indicated that structural and signaling pathways, such as focal adhesion, cytoskeletal organization, and thyroid hormone signaling, are central to the acute-phase response. Consistently, co-expression network analysis reinforced this pattern by identifying cytoskeletal remodeling modules (e.g., *ACTB*, *MYL9*, *ACTN4*, and *COL4A4*), indicating a coordinated transcriptional

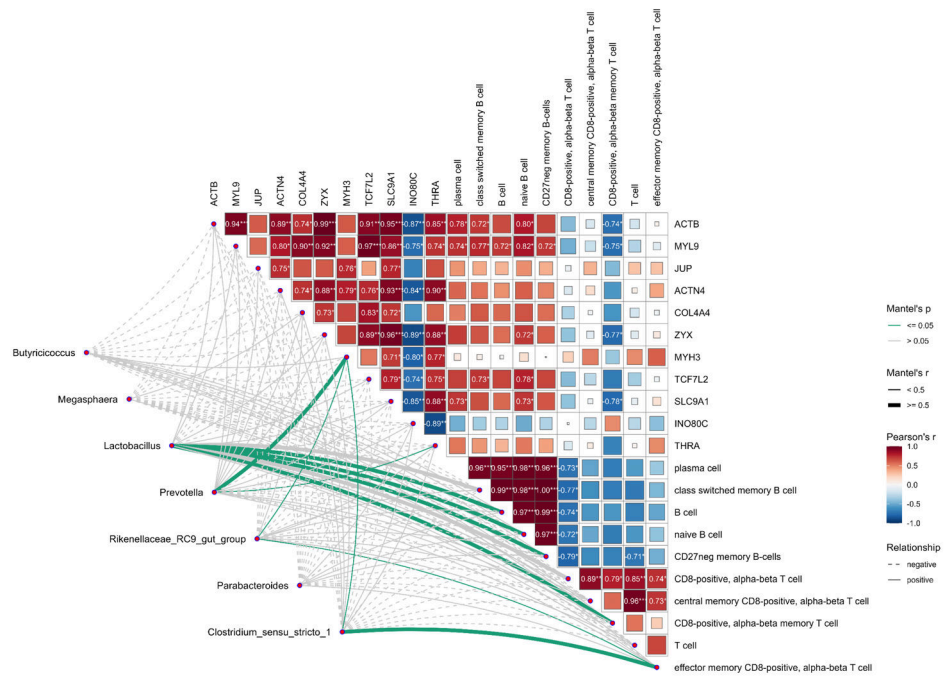


**Fig. 7. Integrated multi-omics correlation framework integrating microbial, transcriptomic, and immune profiles.** In the upper triangular matrix, associations among differentially expressed genes (DEGs) and predicted immune cell types are depicted through Pearson correlation coefficients. Relationships are encoded by a red-to-blue color scale, corresponding to positive and negative correlations. Numerals denote significant associations ( $p < 0.05$ ). The lower triangle summarizes Mantel test outcomes evaluating the global covariation between microbial genera and host-derived transcriptomic or immune profiles. Statistical relevance is represented by line color (green for significant, gray for non-significant), while line types distinguish directionality (solid for positive and dotted for negative interactions).

program aimed at strengthening epithelial integrity under heat stress [48,49].

These transcriptomic changes are accompanied by shifts in immune cell composition. Deconvolution analysis further showed that HS increased T cell and myeloid cell populations, particularly cytotoxic and effector memory subsets, suggesting an acute immune activation profile [50]. In contrast, TN pigs maintained higher levels of B cell subsets, which is consistent with a more stable humoral immune environment [51]. This immune restructuring appears to align with the transcriptomic activation of the migration and adhesion pathways, suggesting the possibility that cellular responses are not only quantitative but also functionally adapted to tissue infiltration and repair [49,52]. Importantly, these parallel findings were not isolated across the omics layers. Indeed, the depletion of *Prevotella* and enrichment of *Clostridium sensu stricto* 1 observed in the microbiome coincided with immune restructuring, wherein TN pigs maintained B-cell subsets, whereas HS pigs shifted toward cytotoxic T-cell dominance. Transcriptomic activation of cytoskeletal genes has been suggested to reinforce the epithelium.

The MOI results of the present study suggest a functional alignment between microbial composition, immune architecture, and host gene expression. Specifically, these results indicated that these patterns converged into two opposing axes: (i) a cytotoxic T cell, *Clostridium sensu stricto* 1 trajectory amplifying inflammatory damage, and (ii) a B cell–*Prevotella*–cytoskeletal trajectory supporting barrier reinforcement. Notably, only the humoral-structural axis formed a coherent functional module that aligned across all omics layers, suggesting that it may represent a recovery-oriented program. These findings are consistent with prior reports showing HS-induced enrichment

of *Clostridium sensu stricto* 1 in pigs [53], further supporting its potential role in exacerbating intestinal inflammation under stress.

Overall, this dual-axis framework provides a mechanistic model for HS acclimation in finishing pigs, moving beyond descriptive observations toward an integrated understanding of host–microbiome–immune interactions. Importantly, this framework indicates that resilience to HS may rely on the host’s capacity to coordinate humoral and structural defenses in partnership with the beneficial microbiota, thereby maintaining barrier integrity and immune balance under stress. Beyond advancing biological understanding, these findings also highlight translational potential. The identified biomarker axis, *Prevotella*, B cells, and cytoskeletal genes, could serve as a foundation for precise strategies to enhance swine thermal tolerance, such as microbiota-targeted interventions or the selection of resilient phenotypes.

## SUPPLEMENTARY MATERIALS

Supplementary materials are only available online from: <https://doi.org/10.5187/jast.2500366>.

## REFERENCES

1. St-Pierre NR, Cobanov B, Schnitkey G. Economic losses from heat stress by US livestock industries. *J Dairy Sci.* 2003;86:E52-77. [https://doi.org/10.3168/jds.S0022-0302\(03\)74040-5](https://doi.org/10.3168/jds.S0022-0302(03)74040-5)
2. Mayorga EJ, Renaudeau D, Ramirez BC, Ross JW, Baumgard LH. Heat stress adaptations in pigs. *Anim Front.* 2019;9:54-61. <https://doi.org/10.1093/af/vfy035>
3. Lambert G, Gisolfi CV, Berg DJ, Moseley PL, Oberley LW, Kregel KC. Selected contribution: hyperthermia-induced intestinal permeability and the role of oxidative and nitrosative stress. *J Appl Physiol.* 2002;92:1750-61. <https://doi.org/10.1152/jappphysiol.00787.2001>
4. Pearce SC, Mani V, Weber TE, Rhoads RP, Patience JF, Baumgard LH, et al. Heat stress and reduced plane of nutrition decreases intestinal integrity and function in pigs. *J Anim Sci.* 2013;91:5183-93. <https://doi.org/10.2527/jas.2013-6759>
5. Huynh TTT, Aarnink AJA, Verstegen MWA, Gerrits WJJ, Heetkamp MJW, Kemp B, et al. Effects of increasing temperatures on physiological changes in pigs at different relative humidities. *J Anim Sci.* 2005;83:1385-96. <https://doi.org/10.2527/2005.8361385X>
6. Renaudeau D, Gourdine JL, St-Pierre NR. A meta-analysis of the effects of high ambient temperature on growth performance of growing-finishing pigs. *J Anim Sci.* 2011;89:2220-30. <https://doi.org/10.2527/jas.2010-3329>
7. Suravajhala P, Kogelman LJA, Kadarmideen HN. Multi-omic data integration and analysis using systems genomics approaches: methods and applications in animal production, health and welfare. *Genet Sel Evol.* 2016;48:38. <https://doi.org/10.1186/s12711-016-0217-x>
8. He J, Guo H, Zheng W, Xue Y, Zhao R, Yao W. Heat stress affects fecal microbial and metabolic alterations of primiparous sows during late gestation. *J Anim Sci Biotechnol.* 2019; 10:84. <https://doi.org/10.1186/s40104-019-0391-0>
9. Ortega ADSV, Szabó C. Adverse effects of heat stress on the intestinal integrity and function of pigs and the mitigation capacity of dietary antioxidants: a review. *Animals.* 2021;11:1135. <https://doi.org/10.3390/ani11041135>
10. Kim M, Roura E, Choi Y, Kim J. Transcriptomic analysis of the porcine gut in response to heat stress and dietary soluble fiber from beet pulp. *Genes.* 2022;13:1456. <https://doi.org/10.3390/genes13081456>
11. Hu C, Patil Y, Gong D, Yu T, Li J, Wu L, et al. Heat stress-induced dysbiosis of porcine

- colon microbiota plays a role in intestinal damage: a fecal microbiota profile. *Front Vet Sci*. 2022;9:686902. <https://doi.org/10.3389/fvets.2022.686902>
12. Schirmer M, Smeeckens SP, Vlamakis H, Jaeger M, Oosting M, Franzosa EA, et al. Linking the human gut microbiome to inflammatory cytokine production capacity. *Cell*. 2016;167:1125-36. <https://doi.org/10.1016/j.cell.2016.11.046>
  13. Ye X, Sahana G, Lund MS, Cai Z. The crosstalk between host and rumen microbiome in cattle: insights from multi-omics approaches and genome-wide association studies. *World J Microbiol Biotechnol*. 2025;41:267. <https://doi.org/10.1007/s11274-025-04504-6>
  14. Hasin Y, Seldin M, Lusis A. Multi-omics approaches to disease. *Genome Biol*. 2017;18:83. <https://doi.org/10.1186/s13059-017-1215-1>
  15. Wang Q, Khatri P, Dinh HQ, Huang J, Pawitan Y, Vu TN. A cluster-based cell-type deconvolution of spatial transcriptomic data. *Nucleic Acids Res*. 2025;53:gkaf714. <https://doi.org/10.1093/nar/gkaf714>
  16. NRC (National Research Council). A guide to environmental research on animals. National Academy of Sciences; 1971.
  17. Xin H, Harmon J. Livestock industry facilities and environment: heat stress indices for livestock. Iowa State University; 1998.
  18. NRC (National Research Council). Nutrient requirements of swine. 11th rev ed. The National Academies Press; 2012.
  19. Bolyen E, Rideout JR, Dillon MR, Bokulich NA, Abnet CC, Al-Ghalith GA, et al. Reproducible, interactive, scalable and extensible microbiome data science using QIIME 2. *Nat Biotechnol*. 2019;37:852-7. <https://doi.org/10.1038/s41587-019-0209-9>
  20. Callahan BJ, McMurdie PJ, Rosen MJ, Han AW, Johnson AJA, Holmes SP. DADA2: high-resolution sample inference from Illumina amplicon data. *Nat Methods*. 2016;13:581-3. <https://doi.org/10.1038/nmeth.3869>
  21. Quast C, Pruesse E, Yilmaz P, Gerken J, Schweer T, Yarza P, et al. The SILVA ribosomal RNA gene database project: improved data processing and web-based tools. *Nucleic Acids Res*. 2012;41:D590-6. <https://doi.org/10.1093/nar/gks1219>
  22. Douglas GM, Maffei VJ, Zaneveld JR, Yurgel SN, Brown JR, Taylor CM, et al. PICRUSt2 for prediction of metagenome functions. *Nat Biotechnol*. 2020;38:685-8. <https://doi.org/10.1038/s41587-020-0548-6>
  23. Parks DH, Tyson GW, Hugenholtz P, Beiko RG. STAMP: statistical analysis of taxonomic and functional profiles. *Bioinformatics*. 2014;30:3123-4. <https://doi.org/10.1093/bioinformatics/btu494>
  24. Brown J, Pirrung M, McCue LA. FQC Dashboard: integrates FastQC results into a web-based, interactive, and extensible FASTQ quality control tool. *Bioinformatics*. 2017;33:3137-9. <https://doi.org/10.1093/bioinformatics/btx373>
  25. Bolger AM, Lohse M, Usadel B. Trimmomatic: a flexible trimmer for Illumina sequence data. *Bioinformatics*. 2014;30:2114-20. <https://doi.org/10.1093/bioinformatics/btu170>
  26. Kim D, Paggi JM, Park C, Bennett C, Salzberg SL. Graph-based genome alignment and genotyping with HISAT2 and HISAT-genotype. *Nat Biotechnol*. 2019;37:907-15. <https://doi.org/10.1038/s41587-019-0201-4>
  27. Li H, Handsaker B, Wysoker A, Fennell T, Ruan J, Homer N, et al. The sequence alignment/map format and SAMtools. *Bioinformatics*. 2009;25:2078-9. <https://doi.org/10.1093/bioinformatics/btp352>
  28. Liao Y, Smyth GK, Shi W. The Subread aligner: fast, accurate and scalable read mapping by seed-and-vote. *Nucleic Acids Res*. 2013;41:e108. <https://doi.org/10.1093/nar/gkt214>

29. Robinson MD, McCarthy DJ, Smyth GK. edgeR: a Bioconductor package for differential expression analysis of digital gene expression data. *Bioinformatics*. 2010;26:139-40. <https://doi.org/10.1093/bioinformatics/btp616>
30. Ritchie ME, Phipson B, Wu D, Hu Y, Law CW, Shi W, et al. Limma powers differential expression analyses for RNA-sequencing and microarray studies. *Nucleic Acids Res*. 2015;43:e47. <https://doi.org/10.1093/nar/gkv007>
31. Dennis Jr. G, Sherman BT, Hosack DA, Yang J, Gao W, Lane HC, et al. DAVID: database for annotation, visualization, and integrated discovery. *Genome Biol*. 2003;4:P3. <https://doi.org/10.1186/gb-2003-4-5-p3>
32. Supek F, Bošnjak M, Škunca N, Šmuc T. REVIGO summarizes and visualizes long lists of gene ontology terms. *PLoS ONE*. 2011;6:e21800. <https://doi.org/10.1371/journal.pone.0021800>
33. Shannon P, Markiel A, Ozier O, Baliga NS, Wang JT, Ramage D, et al. Cytoscape: a software environment for integrated models of biomolecular interaction networks. *Genome Res*. 2003;13:2498-504. <https://doi.org/10.1101/gr.1239303>
34. Bindea G, Mlecnik B, Hackl H, Charoentong P, Tosolini M, Kirilovsky A, et al. ClueGO: a Cytoscape plug-in to decipher functionally grouped gene ontology and pathway annotation networks. *Bioinformatics*. 2009;25:1091-3. <https://doi.org/10.1093/bioinformatics/btp101>
35. Bindea G, Galon J, Mlecnik B. CluePedia Cytoscape plugin: pathway insights using integrated experimental and in silico data. *Bioinformatics*. 2013;29:661-3. <https://doi.org/10.1093/bioinformatics/btt019>
36. Angel A, Naom L, Nabet-Levy S, Aran D. xCell 2.0: robust algorithm for cell type proportion estimation predicts response to immune checkpoint blockade. *bioRxiv*. 2024. <https://doi.org/10.1101/2024.09.06.611424>
37. Witten D, Tibshirani R, Gross S, Narasimhan B, Witten MD. Package 'pma'. *Genet Mol Biol*. 2013;8:28.
38. Huang H. LinkET: everything is linkable. R package version 0.03, GitHub. 2021 [cited 2025 Oct 4]. <https://github.com/Hy4m/linkET>
39. Lu SC. Regulation of glutathione synthesis. *Mol Asp Med*. 2009;30:42-59. <https://doi.org/10.1016/j.mam.2008.05.005>
40. Iwata M, Hirakiyama A, Eshima Y, Kagechika H, Kato C, Song SY. Retinoic acid imprints gut-homing specificity on T cells. *Immunity*. 2004;21:527-38. <https://doi.org/10.1016/j.immuni.2004.08.011>
41. Rajendran V, Kalita P, Shukla H, Kumar A, Tripathi T. Aminoacyl-tRNA synthetases: structure, function, and drug discovery. *Int J Biol Macromol*. 2018;111:400-14. <https://doi.org/10.1016/j.ijbiomac.2017.12.157>
42. Renaudeau D, Collin A, Yahav S, de Basilio V, Gourdiere JL, Collier RJ. Adaptation to hot climate and strategies to alleviate heat stress in livestock production. *Animal*. 2012;6:707-28. <https://doi.org/10.1017/S1751731111002448>
43. Tang S, Xie J, Fang W, Wen X, Yin C, Meng Q, et al. Chronic heat stress induces the disorder of gut transport and immune function associated with endoplasmic reticulum stress in growing pigs. *Anim Nutr*. 2022;11:228-41. <https://doi.org/10.1016/j.aninu.2022.08.008>
44. Vivier E, Tomasello E, Baratin M, Walzer T, Ugolini S. Functions of natural killer cells. *Nat Immunol*. 2008;9:503-10. <https://doi.org/10.1038/ni1582>
45. Flint HJ, Scott KP, Duncan SH, Louis P, Forano E. Microbial degradation of complex carbohydrates in the gut. *Gut Microb*. 2012;3:289-306. <https://doi.org/10.4161/gmic.19897>
46. Koh A, De Vadder F, Kovatcheva-Datchary P, Bäckhed F. From dietary fiber to host

- physiology: short-chain fatty acids as key bacterial metabolites. *Cell*. 2016;165:1332-45. <https://doi.org/10.1016/j.cell.2016.05.041>
47. Hu C, Niu X, Chen S, Wen J, Bao M, Mohyuddin SG, et al. A comprehensive analysis of the colonic flora diversity, short chain fatty acid metabolism, transcripts, and biochemical indexes in heat-stressed pigs. *Front Immunol*. 2021;12:717723. <https://doi.org/10.3389/fimmu.2021.717723>
  48. Prasain N, Stevens T. The actin cytoskeleton in endothelial cell phenotypes. *Microvasc Res*. 2009;77:53-63. <https://doi.org/10.1016/j.mvr.2008.09.012>
  49. Choi Y, Park H, Kim J, Lee H, Kim M. Heat stress induces alterations in gene expression of actin cytoskeleton and filament of cellular components causing gut disruption in growing-finishing pigs. *Animals*. 2024;14:2476. <https://doi.org/10.3390/ani14172476>
  50. Dokladny K, Zuhl MN, Moseley PL. Intestinal epithelial barrier function and tight junction proteins with heat and exercise. *J Appl Physiol*. 2016;120:692-701. <https://doi.org/10.1152/jappphysiol.00536.2015>
  51. Braun RO, Python S, Summerfield A. Porcine B cell subset responses to toll-like receptor ligands. *Front Immunol*. 2017;8:1044. <https://doi.org/10.3389/fimmu.2017.01044>
  52. Geiger B, Spatz JP, Bershadsky AD. Environmental sensing through focal adhesions. *Nat Rev Mol Cell Biol*. 2009;10:21-33. <https://doi.org/10.1038/nrm2593>
  53. Hu C, Niu X, Chen S, Wen J, Bao M, Mohyuddin SG, et al. A comprehensive analysis of the colonic flora diversity, short chain fatty acid metabolism, transcripts, and biochemical indexes in heat-stressed pigs. *Front Immunol*. 2021;12:717723. <https://doi.org/10.3389/fimmu.2021.717723>